Chapter 19

Assessment of Liquefaction Potential

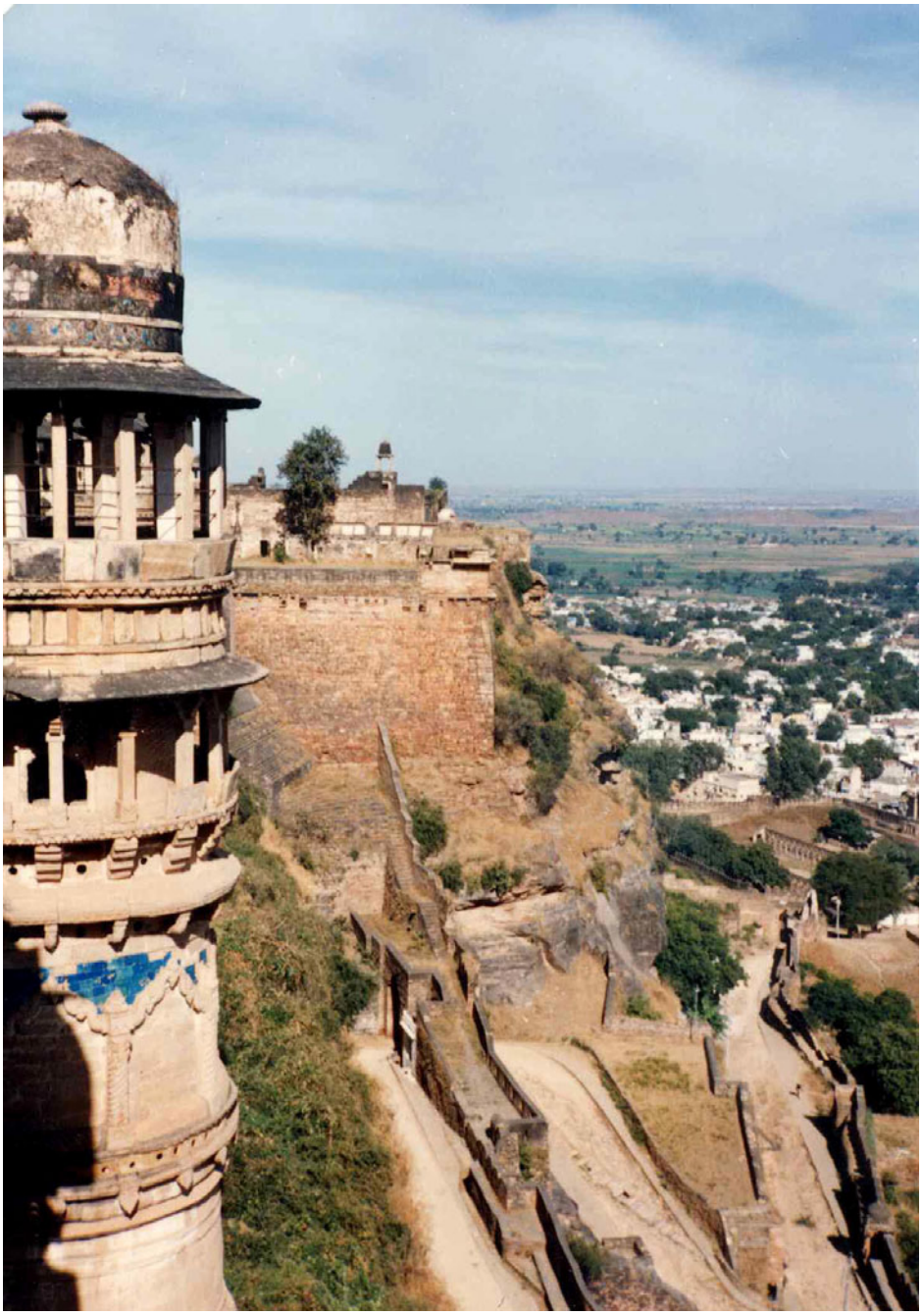

The castle of Gwalior, India.

Many lords or Maha Raja maintained their political status during the British period.

19.1 Significance of Stress Ratio

Resistance of sand against liquefaction is determined by running undrained cyclic triaxial tests on undisturbed soil specimens (Sect. 18.15). Cyclic stress with a constant amplitude is loaded repeatedly (similar to torsion shear tests in Sect. 18.8), and the number of cycles are counted until 1) excess pore water pressure equal to the initial effective stress (σ_c') and (2) peak-to-peak (i.e., double amplitude) axial strain equal to 2.5%, 5%, 10%, etc. The 100% development of excess pore water pressure is called "initial liquefaction" and the strain upon initial liquefaction may not yet be as large as those mentioned above. Thus, liquefaction in laboratory tests are defined in different ways; by pore pressure rise or development of strain. When sand is loose, the number of cycles needed for pore pressure rise and large strain amplitude are not much different.

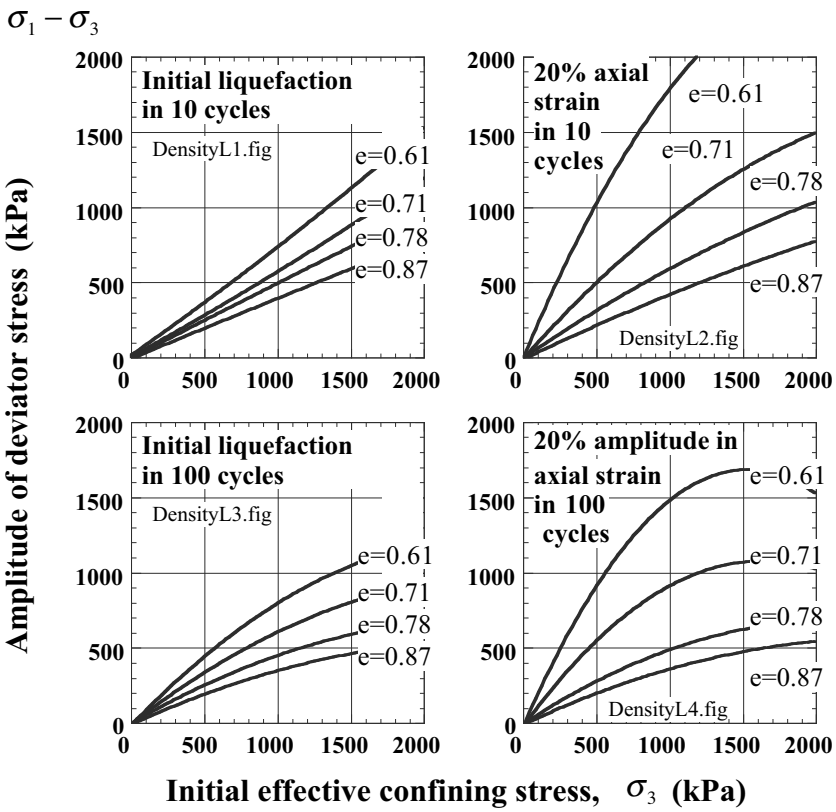

Fig. 19.1 Effects of sand density on stress state to cause liquefaction (Lee and Seed, 1967)

Lee and Seed (1967) reported the cyclic stress amplitude that causes liquefaction in 10 or 100 cycles. In Fig. 19.1, liquefaction is defined by 100% pore pressure rise and 20% axial strain in double amplitude (peak-to-peak amplitude). For any void ratio of sand, the cyclic stress amplitude needed to cause liquefaction increases with the initial confining pressure (consolidation stress). Noteworthy is that the required shear stress amplitude increases as sand becomes denser as well. In Fig. 19.2, the cyclic stress amplitude again increases with the confining pressure. See that liquefaction defined by large strain requires greater stress amplitude than the initial liquefaction defined by pore pressure rise equal to the initial consolidation pressure (initial liquefaction). This means that the strain is not yet large at the moment of initial liquefaction. This is particularly the case of dense sand; see Fig. 19.26.

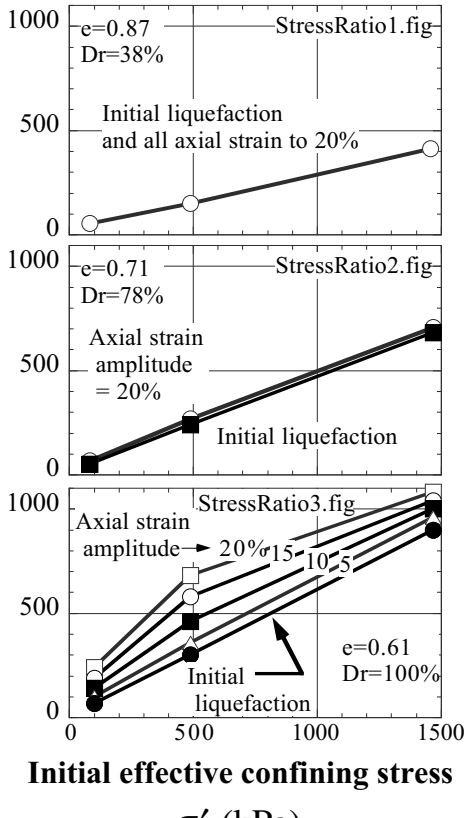

Fig. 19.2 Stress state to cause liquefaction as defined in different ways (Lee and Seed, 1967)

Since the cyclic shear stress increases with the initial confining pressure in these figures, the idea of stress ratio was developed; $\sigma_{dl}/(2\sigma_c')$. Since the stress ratio thus measured stands for the resistance of sand against cyclic undrained loading, it may be called the cyclic resistance ratio (CRR). However, there can be seen in figures some curvature in data. This means that stress ratio needed to trigger liquefaction slightly decreases as effective

stress increases. This is due to negative dilatancy of sand that is more profound under higher pressure (Figs. 1.20 and 1.24). Hence, the resistance of sand against liquefaction, as defined by a cyclic stress ratio, decreases as the overburden pressure (depth) increases, even if other conditions are kept identical.

19.2 Stress Ratio in the Field

Section 19.1 showed that the resistance of soil against liquefaction is expressed by stress ratio, which is measured experimentally by cyclic triaxial tests. In contrast, there is a need to determine the stress ratio that may occur in the field during an expected (design) earthquake. To date, there are two ways to determine this field stress ratio:

1. Use of computer analysis : The wave propagation theory in horizontally layered ground is employed. The design earthquake is specified at the base and an equivalent linear analysis is carried out. The maximum shear stress as calculated is divided by the initial effective vertical stress to obtain τ/σ'_{vc}.

Problem : The equivalent linear analysis does not take into account the softening of soil due to pore pressure build-up. This shortcoming could cause errors in analysis of liquefaction. It is thought today that the equivalent linear analysis is acceptable until apore pressure develops 50%. During this phase, the maximum shear stress is quite likely to occur. Hence, *the field stress that causes liquefaction is able to be predicted by an equivalent linear analysis, but postliquefaction stress and shaking cannot be analyzed.*

2. Use of rigid block analogy : The idea (Seed and Idriss, 1971) is shown in Fig. 19.3. The maximum horizontal acceleration at the ground surface, A_{max}, is directly specified by design codes (for instance, A_{max} = 0.15 G). When the soil column in Fig. 19.3 is ideally rigid, it does not deform and the acceleration is uniformly distributed from the surface to the bottom of the column. By designating the unit weight of soil by γ, the maximum shear stress at the bottom of the column, depth = z, is give by the Newtonian equation of motion 運動方程式;

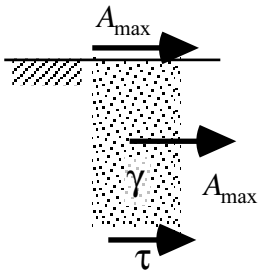

Fig. 19.3 Simple calculation of insitu shear stress

$$\tau = \text{mass of soil column} \times \text{acceleration} = \int_0^z \frac{\gamma}{g} dz \times A_{max} = \sigma_v \frac{A_{max}}{g} \qquad (19.1)$$

in which g stands for the gravity acceleration 重力加速度 =1 G and σ_v is the total vertical stress. Since a level ground is assumed, the lateral earth pressures on the right and left sides of the column are equal to each other and are canceled in the equation of motion. Moreover, the initial effective vertical stress is given by

A typical value of A_{max} is 15–25 % of gravity acceleration.

$$\sigma'_{vc} = \int_0^Z \gamma' dz. \qquad (19.2)$$

Before taking the ratio of shear stress and effective stress as above, a correction for the rigid idealization has to be made. Since the real liquefiable soil is not rigid, shear deformation occurs therein and the acceleration in the soil column is smaller than A_{max} at the surface. Hence, the shear stress at the base of a soil column is smaller than what was calculated as shown earlier. Many dynamic analyses were conducted on a variety of soil conditions and a correction factor of r_d was obtained;

r_d= (maximum shear stress obtained by analysis)
/(shear stress in rigid column)

Figure 19.4 is one of the examples of the calculated range of r_d. In design codes,

$$r_d = 1 - 0.015z \quad \text{or} \quad 1 - 0.025z \tag{19.3}$$

where z is the depth in meter unit (see Sect. 19.11). See also Fig. 19.32. Consequently, the cyclic stress ratio in the field (CSR) is given by

$$\frac{\tau}{\sigma'_{vc}} = r_d \frac{\sigma_v}{\sigma'_{vc}} \frac{A_{max}}{g} \tag{19.4}$$

It is evident that this stress ratio stands for the seismic load, which is in contrast with the resistance of sand against liquefaction (CRR in Sect. 19.1). Note that this stress ratio does not take into account the number of loading cycles and the irregularity of an earthquake motion. In reality, A_{max} which is equivalent with the earthquake loading may be repeated many times if the earthquake magnitude is 7.5 or more, while only a few times when the earthquake magnitude is smaller (see Port Island record, Fig. 18.28). A correction for this shortcoming will be described in Sect. 19.10.

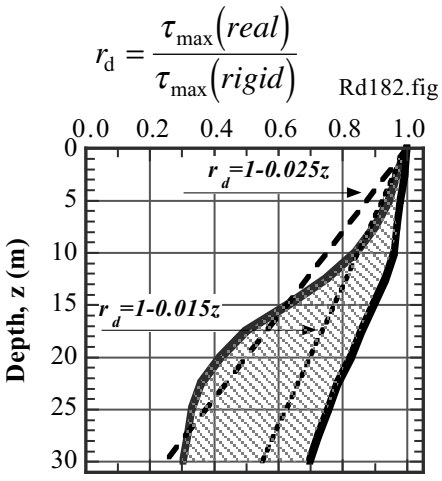

Fig. 19.4 Correction for rigid idealization (original figure by Seed and Idriss, 1971, was revised)

19.3 Liquefaction Curve

The number of loading cycles to liquefaction depends on the amplitude of stress ratio. Therefore, laboratory tests should be run with a variety of stress amplitude, and the varying stress ratio is plotted against the respective number of cycles needed for liquefaction. Liquefaction here is defined by one of the 100% pore pressure development (initial liquefaction), 5%, or greater double (peak-to-peak) amplitudes of axial strain in cyclic triaxial tests. The test data plotted as in Fig. 19.5 is called a liquefaction curve (液状化曲線).

When sand is loose, the number of loading cycles to liquefaction is very similar whether the onset of liquefaction is defined by the 100% excess pore water pressure or large strain amplitude. See Sect. 18.7..

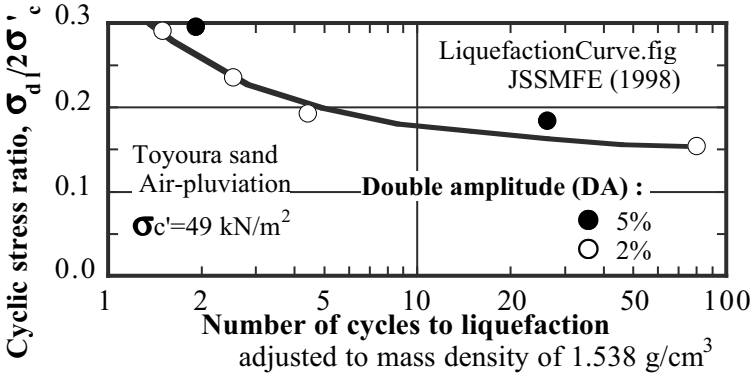

Fig. 19.5 Liquefaction curve of loose Toyoura sand in large triaxial sample; Dr = 65% diameter = 30cm (JSSMFE, 1988)

Figure 19.5 apparently shows that the resistance of sand against liquefaction depends on the number of stress cycles during an expected earthquake. Table 19.1 shows the idea of Seed and Idriss (1982) who replaced an irregular time history of earthquake loading by an equivalent stress history with a constant amplitude. The equivalent stress amplitude is defined by 65% of the maximum shear stress in the irregular history. After this consideration, the number of cycles changing with the earthquake magnitude is taken into account by reducing the soil resistance for quakes of greater magnitude. When an earthquake includes only a few cycles (a case of smaller earthquake magnitude), the soil can resist a greater stress ratio.

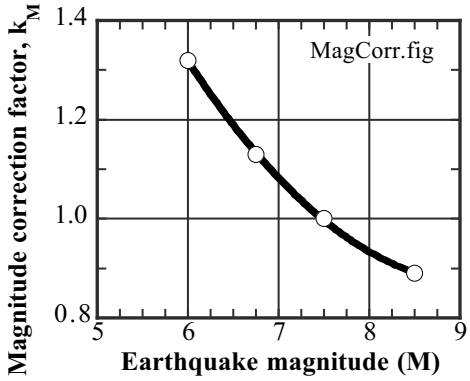

Fig. 19.6 Earthquake magnitude correction of liquefaction resistance (drawn by using Fig. 12 by Seed et al., 1983)

Table 19.1 Equivalent number of cycles (Seed and Idriss, 1982)

Richter scale of earthquake magnitude (M)	Equivalent number of stress cycles (This is a rough estimate.)
8.5	26
7.5	15
6.75	10
6	5–6
5.25	2–3

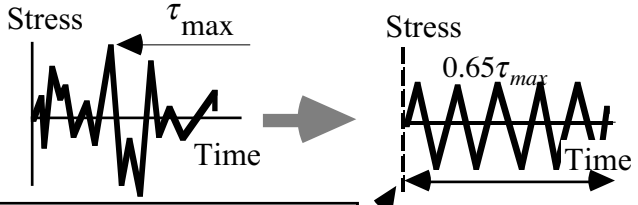

In laboratory tests, sinusoidal wave shape is more common than this triangular wave.

In contrast, when the expected number of cycles is large (an earthquake of larger magnitude), the soil can resist a smaller stress ratio. See the magnitude correction factor, k_M, in Fig. 19.6. Arango (1996) stated that the greater magnitude reduces the minimum acceleration needed for liquefaction because the number of loading cycles is increased.

In today´s practice, the number of equivalent cycles is specified as equal to 20 in most design codes. The seismically induced stress ratio (load) is compared with the stress ratio at 20 cycles in Fig. 19.5 (resistance of soil). Thus, the factor of safety (F_L) is calculated.

The liquefaction curve is drawn on a semilogarithmic plot. Some people prefer to use a log–log plot, because, they insist, the liquefaction curve becomes linear and its analytical expression is easy.

19.4 Field and Laboratory Stress Ratio

When the number of cycles is specified as, for example, 20 (Table 19.1), it is important to compare the resistance of soil against 20 cycles of loading (laboratory stress ratio) and the field stress ratio that is expected to occur during real irregular earthquake loadings.

Factor of safety against liquefaction; F_L = (Resistance: laboratory stress ratio)/(Load: field stress ratio)

These two types of stress ratio include many differences in its nature. Hence, it may not be appropriate to compare them directly and to calculate the factor of safety. A detailed discussion is needed on difference between the laboratory and the field. See Table 19.2 for the idea as well as Fig. 19.7 for definition of stresses. Moreover, the following sections will describe details of the correction parameters.

Table 19.2 Correction of laboratory-measured liquefaction resistance to resistance in field

Issues	Laboratory tri-axial tests	Field conditions	Typical correction factor = Field/Triaxial (reference)
Stress ratio	$\sigma_{dl}/2\sigma_c'$	τ_{max}/σ'_{vc}	----------
Drainage	Undrained	Negligible drainage	Not in practice
Consolidation stress	Isotropic	K_0 consolidation	Use $\tau_{max}/(C_1\sigma'_{vc})$ and $C_1=(1+2K_0)/3$ (Ishihara and Li, 1972)
Number of cycles	Use stress ratio at 20 cycles.	20 is assumed for design	Triaxial sample that can resist 20 cycles of σ_{dl}/σ'_c can resist an irregular loading
Dynamic loading	Mostly sinusoidal	Irregular	with max. $C_2\times(\sigma_{dl}/\sigma'_c)$ where C_2=1/0.65 or 1/(0.55–0.7). (Ishihara and Yasuda, 1975)
Sheared plane	Inclined 45°, cone shaped	Horizontal and planar	Not in practice; anisotropy may affect
Stress axes	Fixed vertical axis	Rotation around	Not in practice; anisotropy may affect
Sample disturbance	Resistance is underestimated		Use $C_3\times(\sigma_{dl}/2\sigma'_c)$ and C_3>1 but not clearly understood yet
Sand density	Densified during handling	Weaker than laboratory tests	Use $C_4\times(\sigma_{dl}/2\sigma'_c)$ and C_4<1 but not clearly understood yet
Cyclic change of stress	Only axial stress: overestimation of strength	At least 2 components; EW and NS.	Use $C_5\times(\sigma_{dl}/2\sigma'_c)$ and C_5=0.8–0.9 or more (Ishihara and Yamazaki, 1980)
Saturation	Saturated; B > 0.95	Not saturated? difficult to know	Not in practice; probably C < 1

The Japanese Design Code of Highway Bridge 道路橋示方書 V 耐震設計篇, which is one of the most important codes concerning liquefaction, states that, when K_0=0.5, $C_1 \times C_2$ is approximately equal to one. Moreover, $C_3 \times C_4 = 1$ is assumed, although the quality of samples is unpredictable. By further assuming $C_5 = 1$, accordingly, $C_1C_2C_3C_4C_5 \cong 1$ and

$$F_{\mathrm{L}} = \frac{\text{Triaxial strength}}{\text{Field stress ratio}} = \frac{C_2C_3C_4C_5\left\{\sigma_{\mathrm{dl}}/\left(2\sigma'_{\mathrm{c}}\right)\right\}_{\text{triaxial}}}{\left(\tau_{\max}/C_1\sigma'_{\mathrm{vc}}\right)_{\text{field}}} = \frac{\left\{\sigma_{\mathrm{dl}}/\left(2\sigma'_{\mathrm{c}}\right)\right\}_{\text{triaxial}}}{\left(\tau_{\max}/\sigma'_{\mathrm{vc}}\right)_{\text{field}}} \tag{19.5}$$

Thus, the laboratory stress ratio obtained by cyclic triaxial test is directly compared with the field stress ratio. Note that this F_{L} indicates the liquefaction potential of a single soil layer from which the tested sample was collected. It does not indicate the risk of liquefaction damage of a site. The liquefaction damage risk depends on the total thickness of liquefied layer as well.

Commonly encountered questions addresses the effects of initial static shear stress, that may cause large distortion of subsoil, the effects of different earthquake magnitudes that may produce different number of loading cycles, and the level of confining pressure (depth). For these issues, refer to Sects. 19.6, 19.3, and 19.9, respectively.

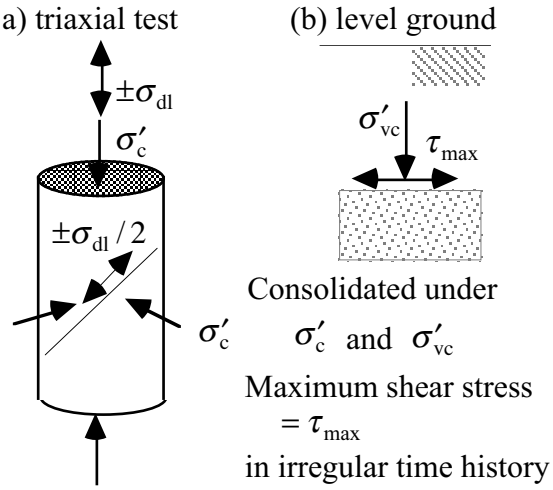

Fig. 19.7 Stress states in triaxial tests and horizontal shaking of level ground

19.5 Effects of Static Shear Stress on Resistance Against Liquefaction

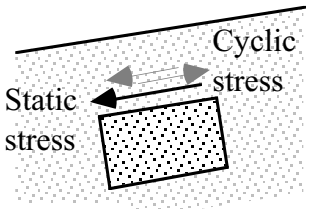

Fig. 19.8 Initial shear stress in a slope

Cyclic triaxial tests on liquefaction resistance of sand (Sect. 18.15) are carried out on isotropically consolidated samples in which there is no static shear stress. This means that liquefaction in level ground is studied. Then a question arises; what is the liquefaction potential of slopes where there is an initial static shear stress and it is superimposed by cyclic shear stress (Fig. 19.8).

The effects of the static shear stress on undrained behavior of sand are illustrated in Figs. 19.9 and 19.10. In Fig. 19.9, the static shear stress of 20 kPa was applied in a drained manner and was then superimposed by a cyclic component of ±20 kPa in a torsion shear apparatus (Sect. 18.8). Hence, the combined shear stress (static + cyclic) changed between 0 and +40 kPa. Since the stress was always positive (or zero), this type of loading was called one-way (片振り). Although so many cycles of shear stress were loaded, the sample maintained its stability. In Fig. 19.10, in contrast, the cyclic component had a greater amplitude of ±30 kPa, making the combined stress vary between –10 and +50 kPa. This type of loading was called two-way (両振り). The specimen easily liquefied and developed large shear deformation. Note that two-way loading is very important in causing liquefaction under effects of static shear stress.

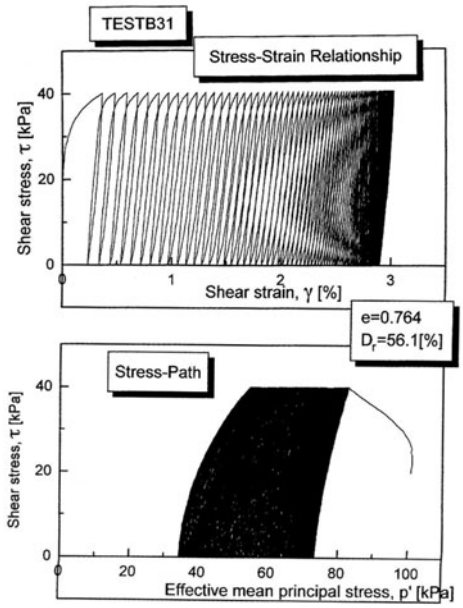

Fig. 19.9 One-way test loading on sample with the relative density of 56.1% (Yokouchi, 1997)

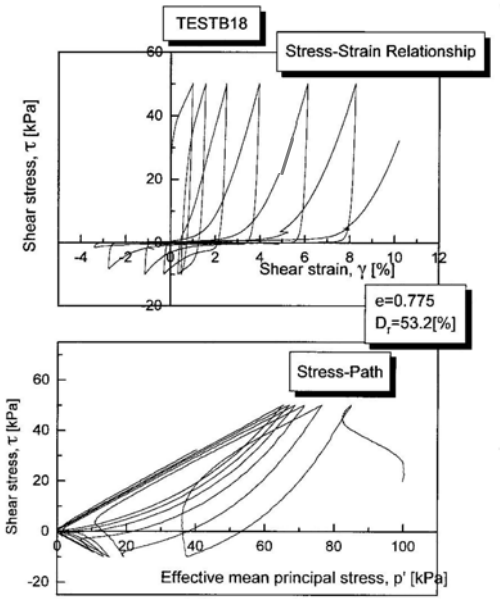

Fig. 19.10 Two-way loading on sample with the relative density of 53.2% (Yokouchi, 1997)

When the static shear stress is substantial, the combined stress (static + cyclic) is unlikely to be zero (one-way loading). Therefore, liquefaction (effective stress = 0, shear stress = 0) is difficult to occur. This, however, does not mean that sand is very resistant against seismic loading. A significant magnitude of combined shear stress may cause shear failure. It is, therefore, important to watch whether or not the effective stress state comes close to the failure criterion ($\tau = \sigma' \tan\phi$). If the failure criterion is nearly satisfied, shear strain of a few % or more is possible to occur. This point is particularly important in very loose sand, which is subjected to a disastrous flow failure (see, for example, Sect. 24.3).

In another undrained torsion shear test in Fig. 19.11(a), (1) the deviator stress ($\sigma_1 - \sigma_3$) was loaded to a specified value (C→A), (2) orientations of σ_1 and σ_3 rotated over ±45° with constant $\sigma_1 - \sigma_3$ until large shear deformation occurred (A→B), and then (3) $\sigma_1 - \sigma_3$ was unloaded to zero (B→O). Although P' and pore water pressure stopped its variation at the end of Stage 2 (Point B), they started to change again in

the unloading phase (Stage 3 after B). The variation and motion of Mohr stress circle is illustrated in Fig. 19.12. At B, Mohr effective stress circle touched the failure envelope and large strain started to develop, Fig. 19.11(b). Thereinafter, $\sigma_1 - \sigma_3$ was reduced and the excess pore water pressure increased quickly; the specimen liquefied. It is reasonable, therefore, that shear stress near failure prevents further pore pressure rise with the aid of positive dilatancy. In other words, the Mohr stress circle at B is in contact with the failure line and cannot translate toward the left any more. When this effect disappears, liquefaction is quite likely (Stage 3).

(a) Decrease of effective stress with rotation of stress axis

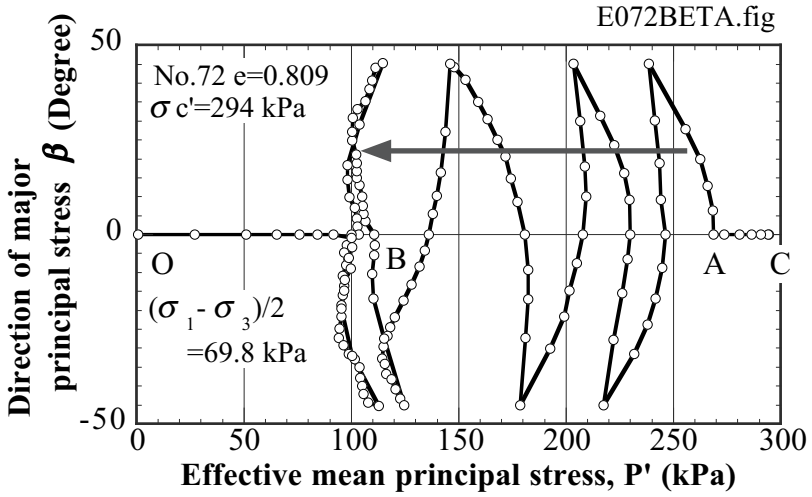

(b) Development of strain with rotation of stress axis

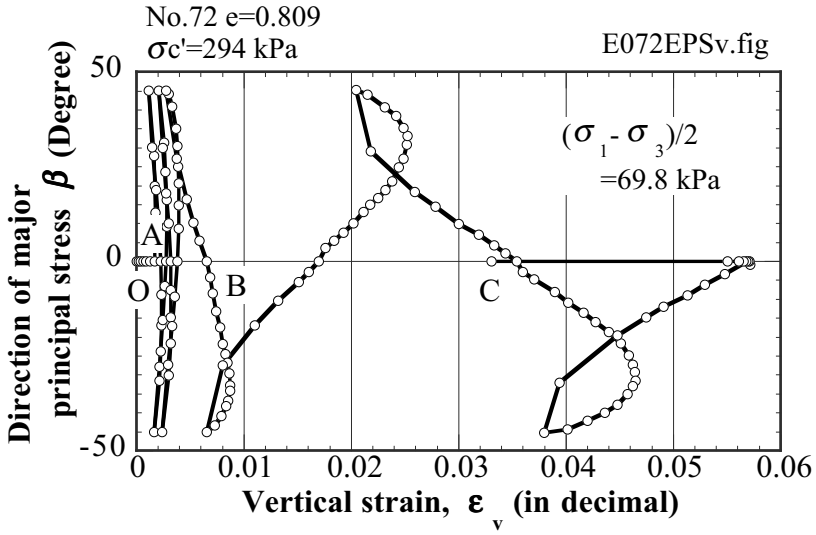

Fig. 19.11 Undrained torsion shear with constant deviator stress

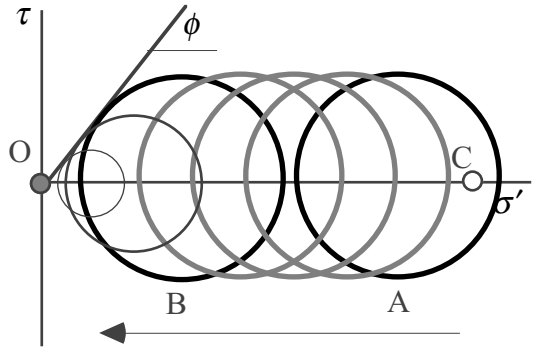

Fig. 19.12 Behavior of Mohr effective stress circle during test in Fig. 19.11

19.6 Importance of Two-Way Loading in Cyclic Shear with Initial Static Stress

The study on initial static shear started from an interest in seismic stability of slopes and embankments. By assuming that a slip plane coincides with the 45° plane in a triaxial specimen (Fig. 19.13), triaxial shear tests on anisotropically consolidated specimen (3.5 in. high) were conducted. After consolidation under $K_c = \sigma'_{1c}/\sigma'_{3c}$, a cyclic deviator stress, $\pm\sigma_{dl}$, was loaded (Lee and Seed, 1967).

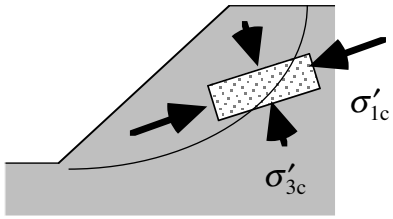

Fig. 19.13 Modelling seismic failure of slope by triaxial test

In the test of Fig. 19.14, a specimen of Sacramento River sand with D_r = 38% was loaded under σ'_{1c} = 196 kN/m^2 and σ'_{3c} = 98 kN/m^2, while the cyclic deviator stress varied between σ_{dl} = 102 and –94 kN/m^2. Hence, the combined axial stress was between 298 and 102 kN/m^2 and was always greater than the lateral stress. This one-way test is also called nonreversal. Figure 19.14 shows that the axial deformation increased very slowly and the excess pore water pressure never reached σ'_{3c}. On the contrary in Fig. 19.15, the amplitude of the deviator stress was ±102 kN/m^2. Although the maximum combined shear stress was same as in Fig. 19.14, the minimum stress was –4 kN/m^2. This slight reversal of shear stress direction (negative deviator stress) made a drastic difference in soil behavior. Figure 19.15 reveals that the sample liquefied quickly.

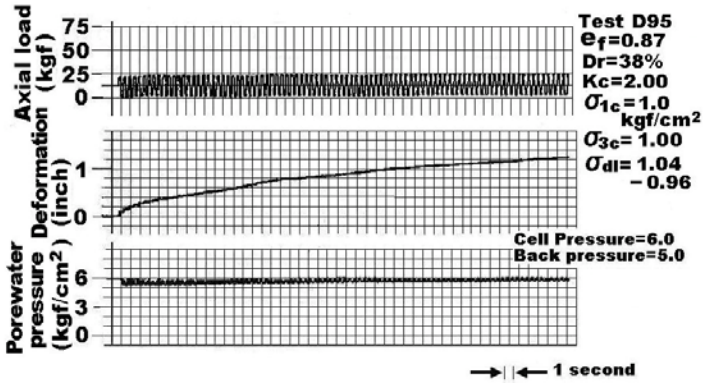

Fig. 19.14 Cyclic undrained shear without stress reversal (Seed and Lee, 1967)

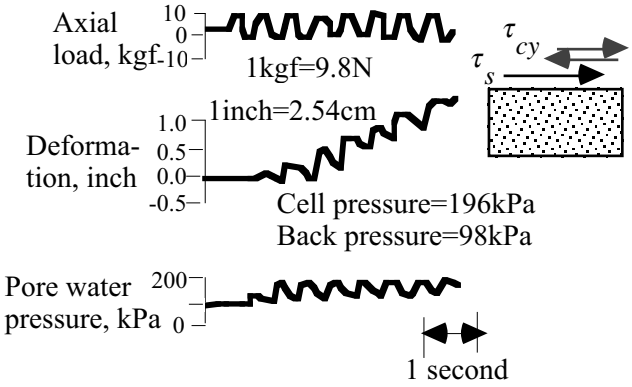

Fig. 19.15 Cyclic undrained shear with stress reversal (after Seed and Lee, 1967)

Vaid and Finn (1967) carried out simple shear tests (as schematically shown in inset figure in Fig. 19.15) on Ottawa sand, which was of Dr = 50% and was consolidated under σ'_{vo} = 196 kN/m^2. Figure 19.16 shows that the cyclic stress ratio, τ_{cy}/σ'_{vo}, needed to develop strain of γ = 2% at 10th cycle decreased as the static stress ratio τ_{max}/σ'_{vo} increased. It seems that static shear makes small strain easy to develop. Conversely, τ_{cy}/σ'_{vo} required for γ = 10% increased. More significant positive dilatancy due to greater static shear prevents a large

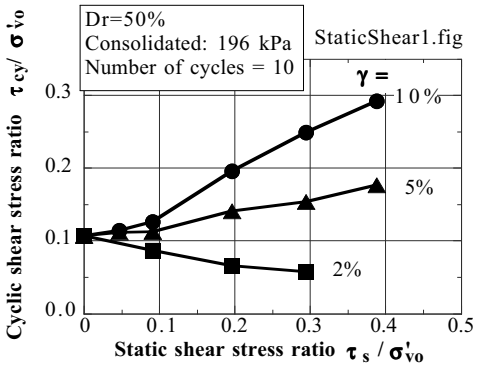

Fig. 19.16 Effects of static shear on cyclic component of strength (after Vaid and Finn, 1979)

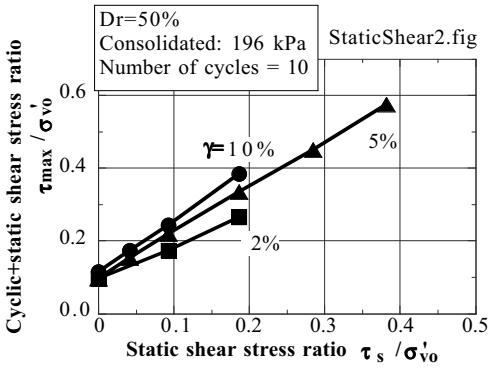

Fig. 19.17 Effects of static shear on combined strength of sand (after Vaid and Finn, 1979)

strain to develop. The combined stress ratio in Fig. 19.17, $\left(\tau_{\max} = \tau_{\mathrm{s}} + \tau_{\mathrm{cy}}\right)\big/\sigma'_{\mathrm{vo}}$ increases as the initial static stress increases. This means that the cyclic strength of sand is increased by the static shear. The correction factor for the initial static shear stress, k_{a}, was proposed to take this issue into account and increase the liquefaction resistance obtained experimentally without static shear stress (Federal Highway Administration, 1997). Note that the discussion so far made is based on strain amplitude induced by cyclic loading. In case of very loose sand subjected to static shear, large residual deformation and flow failure are more important issue; see Chap. 24.

19.7 Effects of K_0 Consolidation on Liquefaction Resistance of Sand

Cyclic triaxial test is useful in practice because it can test undisturbed soil samples. Conversely, one of its drawbacks is the different stress states during consolidation; isotropic consolidation in triaxial tests and K_0 consolidation in real subsoil. K_0 consolidation in level ground is characterized by (see Fig. 18.51)

1. The different effective stress in the horizontal and vertical directions; $\sigma'_h = K_0\sigma'_v$
2. Lateral deformation is not allowed during consolidation and during cyclic shear

In the sense of (2), K_0 consolidation is discriminated from anisotropic consolidation which is the case under shallow foundation, embankments, etc. Simple shear of a box-shape specimen can best reproduce the state of K_0 consolidation, although it cannot test undisturbed specimens and produces a nonuniform stress state within a specimen (Cole, 1967).

Finn et al. (1971) compared stress ratio obtained by triaxial and simple shear tests (Fig. 19.18). They concluded that two types of stress ratio are related with each other by

$$\frac{\sigma_{dl}}{2\sigma'_{co}} = \frac{\text{Cyclic shear stress}}{\text{Mean consolidaiton stress}} = \frac{\tau_{cy}}{\frac{1+K_0}{2}\sigma'_{vo}}$$

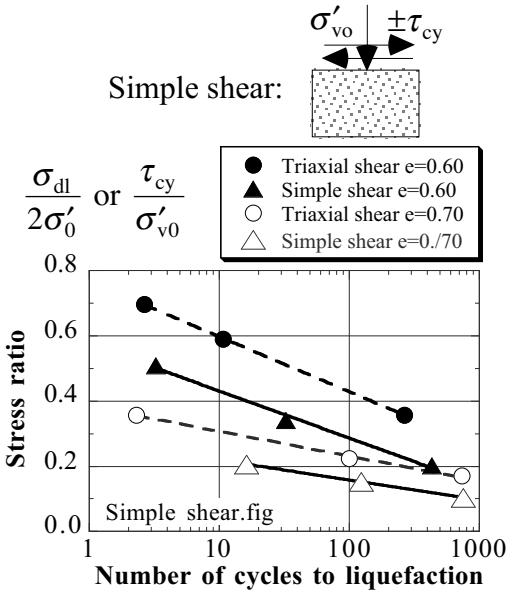

Fig. 19.18 Different liquefaction resistances obtained by simple shear and triaxial shear (Finn et al., 1971)

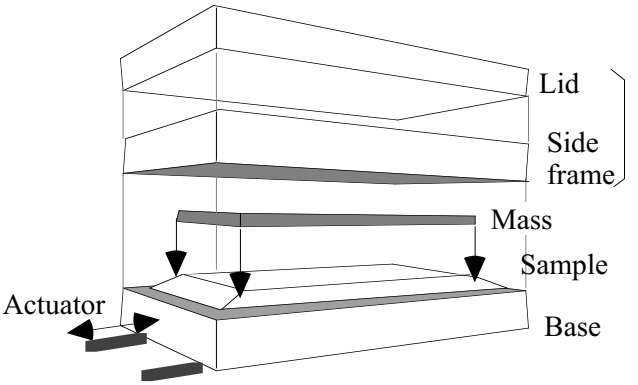

Fig. 19.19 Large simple shear device excited on shaking table (after De Alba et al., 1976)

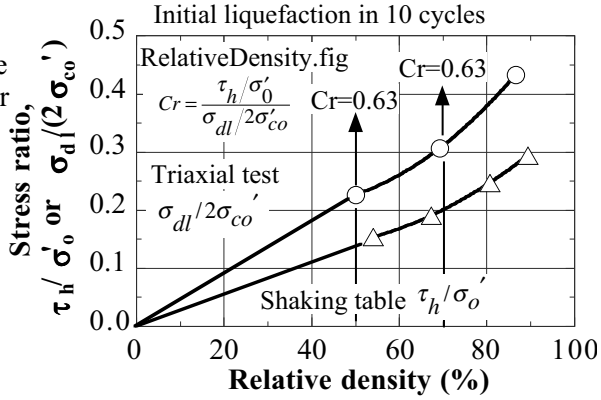

Fig. 19.20 Comparison of liquefaction resistance of sand obtained by triaxial and simple shear tests (after De Alba et al., 1976)

De Alba et al. (1976) carried out shaking table tests (Fig. 19.19) in which a layer of sand covered by a rubber sheet was consolidated by air pressure and sheared by force generated by a shaking top mass (shear force = mass × acceleration). The liquefaction resistance (stress ratio required for initial liquefaction at 10th cycle, in which initial liquefaction means the excess pore pressure reaching the consolidation pressure) obtained by triaxial tests and this simple shear is examined in Fig. 19.20. Eventually, a conversion formula of

$$\frac{\sigma_{dl}}{2\sigma'_{co}} = \frac{\tau_{cy}}{C_1\sigma'_{vo}} \text{ where } C_1 \approx 0.63$$

was proposed between two kinds of stress state.

19.8 Liquefaction Resistance of Sand Under K_0 Condition and Overconsolidation

The K_0 condition of a level ground is characterized by the lateral confinement in which the horizontal strain, ε_h, is held zero during shaking. This means that no horizontal extension or contraction occurs in the subsoil, although horizontal displacement is excited by shaking. Since a level ground is idealized by an infinite size, even the smallest ε_h gives an infinite displacement when it is multiplied by an infinite size. Therefore, the strain has to be zero.

The idea of earth pressure at rest states that the ratio of horizontal and vertical effective stresses are kept equal to K_0 when ε_h is zero. By denoting the hydrostatic pore pressure and excess pore water pressure by u_s and Δu, respectively, the ratio of total stress is derived:

$$\frac{\sigma_h}{\sigma_v} = \frac{\sigma'_h + u_s + \Delta u}{\sigma'_v + u_s + \Delta u} = \frac{K_0\sigma'_v + u_s + \Delta u}{\sigma'_v + u_s + \Delta u} \qquad (19.6)$$

This means that, when σ'_v is reduced to zero upon liquefaction, the total stress ratio becomes equal to one, which stands for an isotropic stress state.

Table 19.3 indicates the change of stress components and Fig. 19.21 illustrates the variation of Mohr's effective stress circle during liquefaction procedure, while Fig. 19.22 reveals the variation of total and effective stress states. Note that the stress difference, $\Delta\sigma_1 - \Delta\sigma_3$ decreases.

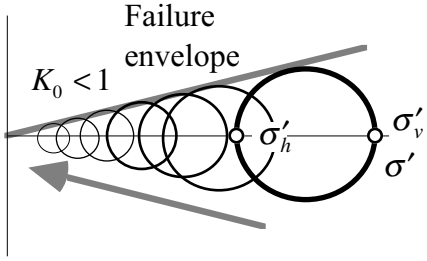

Fig. 19.21 Effective stress circle during liquefaction process

Table 19.3 Change of stress components during liquefaction process

	Total stress		Effective stress	
	$\sigma_1 = \sigma_v$	$\sigma_1 = \sigma_h$	σ'_v	σ'_h
Initial	$\sigma_1 = \sigma_{vo}$	$\sigma_3 = K_0\sigma'_{vo} + u_s$	σ'_{vo}	$K_0\sigma'_{vo}$
Upon liquefaction	$\sigma_1 = \sigma_{vo}$	$\sigma_3 = \sigma_{vo} = \sigma'_{vo} + u_s$	0	0

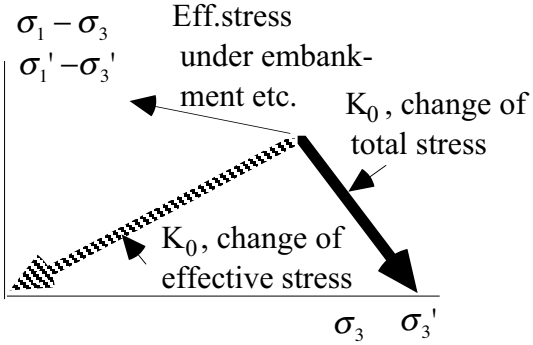

Fig. 19.22 Change of total stress state during liquefaction process

The excess pore water pressure is generated not only by cyclic shear but by the total stress change. The latter component may be given by modifying Skempton´s formula:

$$\Delta u_t = B\Delta\left(\frac{\sigma_1 + 2\sigma_3}{3}\right) + A\left(\Delta\sigma_1 - \Delta\sigma_3\right) \qquad (19.7)$$

Since $\Delta\sigma_1 - \Delta\sigma_3$ is unloaded (decrease) during the process of liquefaction (Table 19.3), it does not develop much pore pressure; see the stress path of unloading phase in Fig. 18.17. Hence, A = 0 is reasonable. Moreover, B = 1 in water saturated sand. Therefore,

$$\Delta u_t = \frac{2}{3}\left(1 - K_0\right)\sigma'_{vo} \qquad (19.8)$$

Ishihara and Li (1972) stated that stress ratio should be defined as the ratio of cyclic shear stress

amplitude over excess pore water pressure generated by cyclic loading, while excluding Δu_t (19.7). In K_0 condition, therefore,

$$\text{Stress ratio} = \frac{\tau_{cy}}{\sigma'_{vo} - \Delta u_t} = \frac{\tau_{cy}}{\sigma'_{vo} - \frac{2}{3}(1 - K_0)\sigma'_{vo}} = \frac{\tau_{cy}}{\frac{1+2K_0}{3}\sigma'_{vo}} \qquad (19.9)$$

which is equivalent with the stress ratio of triaxial test;

$$\frac{\sigma_{dl}}{2\sigma'_{co}} = \frac{\tau_{cy}}{\frac{1+2K_0}{3}\sigma'_{vo}} \quad \text{and hence,} \quad C_1 = \frac{1+2K_0}{3} \qquad (19.10)$$

in Sect. 19.4. C_1 is *0.67* for a typical value of $K_0 = 0.5$.

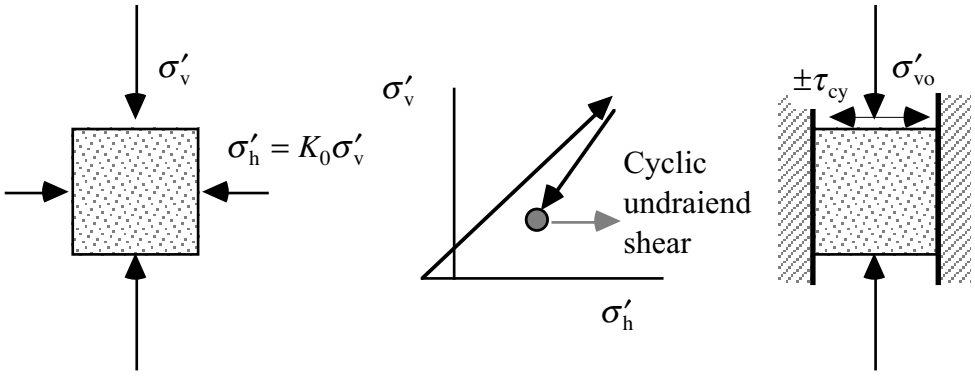

Fig. 19.23 Stress history in torsional shear tests on overconsolidated sand

Overconsolidated stress state increases liquefaction resistance of sand in two manners. First, overconsolidated level ground is of greater K_0 value (earth pressure coefficient at rest), which is defined by (horizontal effective stress)/(vertical effective stress, σ'_v) (19.23). This is due to plastic deformation of sand in the horizontal direction during the preceding high vertical stress. To reduce the horizontal expansion, the horizontal effective stress has to be maintained high after unloading of σ'_v, leading to greater K_0. Second, the stress history of overconsolidation makes sand less contractive (or more dilative) during cyclic shear. Hence, excess pore water pressure develops less during cyclic undrained shear.

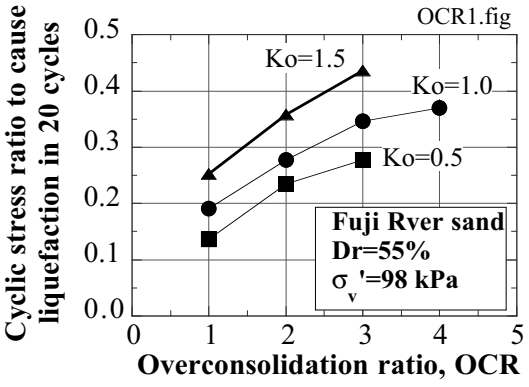

Fig. 19.24 Increase of liquefaction resistance of sand due to overconsolidation (Ishihara and Takatsu, 1979)

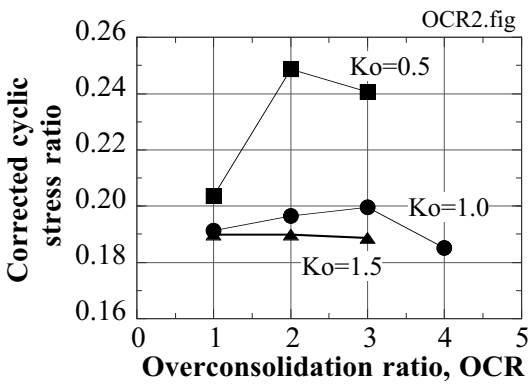

Fig. 19.25 Normalized cyclic stress ratio to cause liquefaction in 20 cycles (data by Ishihara and Takatsu, 1979)

Ishihara and Takatsu (1979) carried out undrained torsional shear (Fig. 19.24) to study the overconsolidation effects on liquefaction. The stress state in this device is illustrated in Fig. 19.23. Specimens were subjected to stress history of loading and unloading so that the desired overconsolidation ratio (*OCR*) was produced. In this stage, the ratio of K_0 was maintained constant. Thereinafter, cyclic shear stress, τ, was loaded in an undrained manner, while preventing lateral deformation from occurring. This situation is similar to what happens in real level ground.

Figure 19.24 compares stress ratio, (τ_{cy}/σ'_{vo}), which was needed to cause liquefaction in 20 cycles. Evidently, the stress ratio (resistance of sand against liquefaction) increases with both K_0 and overconsolidation ratio. It was then attempted to express the effects of these parameters by using such an empirical formula as

$$\left(\frac{\tau_1}{\sigma'_{vo}}\right)_{OC,K_0} = \frac{1+2K_0}{3}\sqrt{OCR}\left(\frac{\tau_1}{\sigma'_{vo}}\right)_{NC,K_0=1} \quad (19.11)$$

The stress ratio thus corrected is plotted in Fig. 19.25. Although some data are still different, there is a general consistency. On the basis of these findings, it may be reasonable to state that liquefaction resistance of sand is improved by producing overconsolidated stress state by means of preloading.

19.9 Effects of Confining Pressure on Liquefaction Resistance

Monotonic shear of sand under different consolidation pressures reveal that higher pressures make sand more contractive during shear than lower pressures (Fig. 1.17). The same is true of liquefaction because the development of excess pore water pressure is a consequence of (negative) dilatancy; see Sects. 18.1 or 20.1. Hence, liquefaction is more likely under higher consolidation stresses.

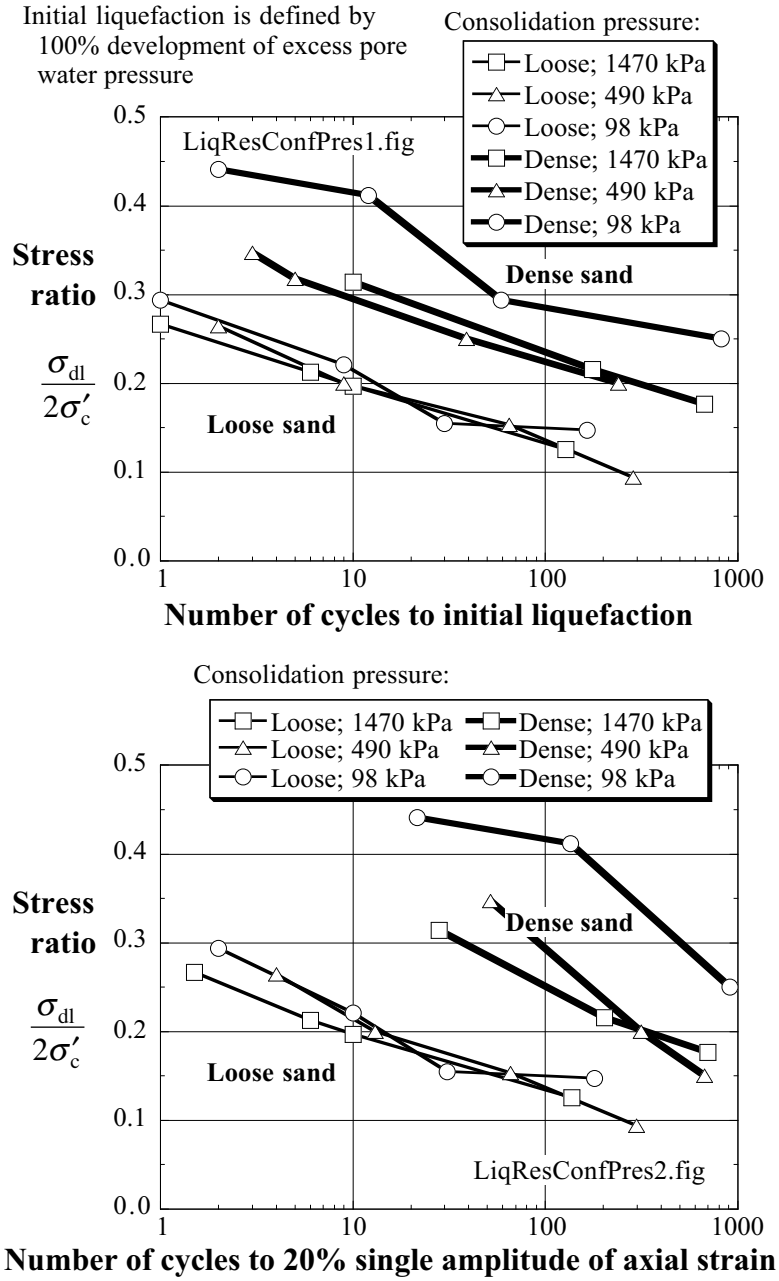

Fig. 19.26 Cyclic triaxial test data on liquefaction resistance of sand under different stress levels (reproduced from data by Seed and Lee, 1967)

Figure 19.26 was drawn by the author by using a pioneering data set by Lee and Seed (1967). The employed sand was uniform Sacramento River sand with e_{max} and e_{min} = 1.03 and 0.63, respectively. The relative density of loose and dense sands were 30% and 78%. The amplitude of cyclic axial stress in the original paper was converted to the cyclic stress ratio according to the present convention.

It appears evident, particularly for dense sand, that higher consolidation pressure, σ'_c, reduces the stress ratio needed for liquefaction, whether liquefaction is defined by 100% pore pressure rise or large axial

strain. Similar finding was reported later by Vaid and Chern (1985). This issue is taken into account by what is called the correction factor for stress levels, k_σ (Federal Highway Administration of USA, 1997).

From such a discussion, some people imagine that insitu sand at greater depth is more vulnerable to liquefaction than sand near the surface, because the greater depth means higher consolidation pressure. It is not true, however, because sand at a greater depth is more aged and the liquefaction resistance of sand increases with the number of years after deposition. This is called ageing effects. See Sect. 18.13.

19.10 Effects of Irregular Loading on Resistance Against Liquefaction

Resistance of sand against liquefaction is conventionally indicated by the stress ratio that causes liquefaction (Sect. 19.3), whether 100% pore pressure development or significant strain amplitude, at 20 cycles of constant amplitude. The real earthquake loading, however, has never a constant stress amplitude or 20 cycles. It seems that the idea of "20" cycles empirically comes from a rule of thumb shown in Table 19.4.

Table 19.4 Equivalent number of cycles (after Seed and Idriss, 1971).

Earthquake magnitude (Richter scale)	Number of significant stress cycles
7	10
7.5	20
8	30

The effect of irregular loading was studied by running torsion shear tests on isotropically consolidated specimens with D_r = 55% (Ishihara and Yasuda, 1975). Figure 19.27 illustrates results of a test in which a time history of Hachinohe NS record during the 1968 Tokachi-oki earthquake (Fig. 5.9) was loaded. Note that this record has a few stress cycles with relatively large stress amplitudes, while other cycles are of minor magnitudes. Hence, this record is classified as "a shock type (衝撃型)." By varying the maximum stress, τ_{max}, while maintaining the wave shape unchanged, the minimum value of τ_{max} needed for liquefaction was determined. This amplitude is called τ_{cy} in this section. See Fig. 19.28 for illustration.

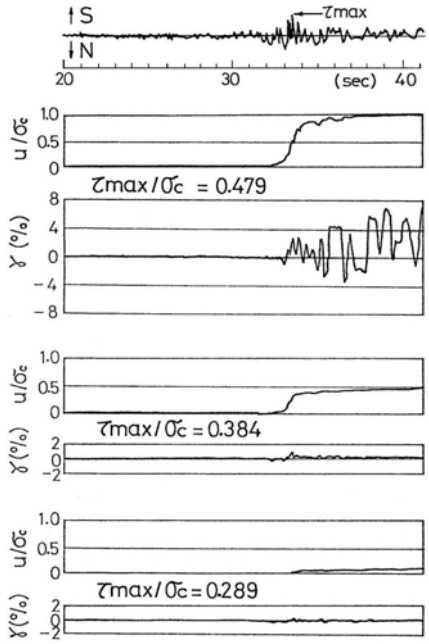

Fig. 19.27 Liquefaction test with Hachinohe NS record (Ishihara and Yasuda, 1975)

Similar tests were conducted on Aomori record in Fig. 19.29. This record is characterized by many cycles of stress, which are of major magnitudes. Hence, this type of record is called "vibratory type (振動型)."

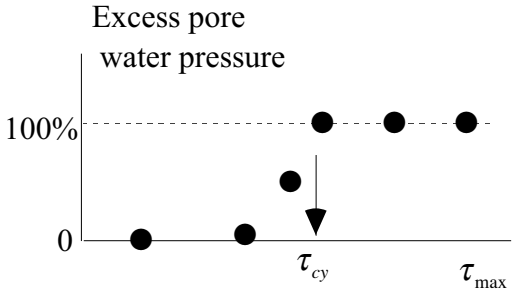

Fig. 19.28 Idea of liquefaction resistance under irregular loading

Similar tests were further conducted with four more records so that the liquefaction resistance under irregular loading thus determined, τ_{cy}, was compared with the liquefaction resistance in triaxial tests on isotropically consolidated specimens. The correction factor, C in Sect. 19.4, for irregularity was obtained as manifested below; [2]

$$\frac{\tau_{cy}}{\sigma'_{vo}} = C_2 \frac{\sigma_{dl}}{2\sigma'_{co}} \quad \text{and}$$

Shock type: only 0–2 cycles before occurrence of τ_{max} have amplitudes greater than 60% of τ_{max} $\rightarrow C_2$=1/0.55.

Vibratory type: 3 or more than 3 cycles before occurrence of τ_{max} have amplitudes greater than 60% of τ_{max} $\rightarrow C_2$= 1/0.70.

Seed and Idriss (1971) proposed to use C_2= 1/0.65 by engineering judgment.

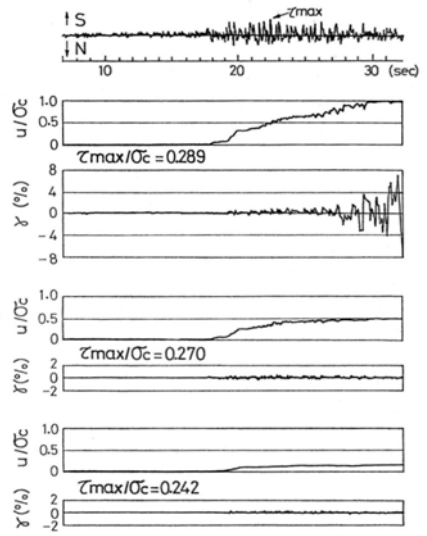

Fig. 19.29 Liquefaciton test with Aomori NS record (Ishihara and Yasuda, 1975)

Another approaches to assess the liquefaction potential under irregular stress time history is the use of accumulated damage concept (累積損傷). Originally developed in the field of fatigue failure of metals, this approach evaluates contribution to liquefaction of each stress cycle (Lee and Chan, 1972). For example in an irregular time history in Fig. 19.30, the first stress cycle has a stress ratio amplitude of SR_1. Since the liquefaction strength test implies that this stress ratio requires $N_{L,1}$ cycles to liquefaction, this stress cycle makes $(1/N_{L,1})$ contribution to the onset of liquefaction. Similarly, another cycle of SR_2 makes a contribution of $(1/N_{L,2})$. Consequently, the entire stress ratio history makes a total contribution of $\sum_i \left(1/N_{L,i}\right)$. If this total contribution exceeds 1.0, liquefaction is quite likely to occur. Considering anisotropic nature of soil and different magnitudes of stress between positive and negative directions, Annaki and Lee (1977) proposed to do the above calculation for each half cycle. Note that this idea does not consider the elastoplastic nature of soil in which the order of lower and higher stress affects elastic and plastic behavior of soils.

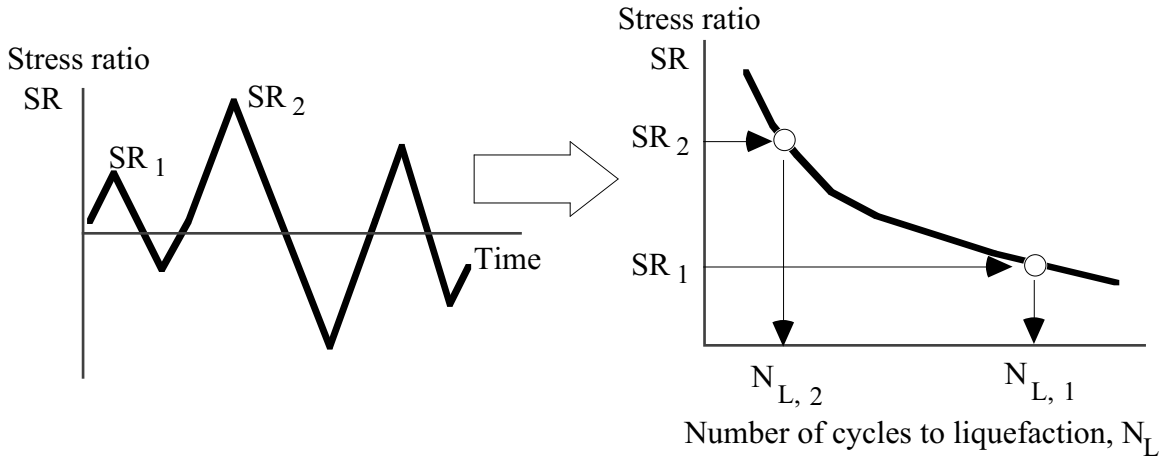

Fig. 19.30 Contribution to liquefaction of individual stress cycle

19.11 Correction of Stress Ratio with Depth

When one calculates the factor of safety against liquefaction, the amplitude of cyclic shear stress is approximately assessed by

$$\tau_{cy} = \frac{A_{max}}{g}\left(\text{weight of soil}\right) \times r_d \qquad (19.12)$$

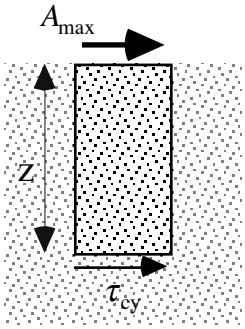

Fig. 19.31 Shear stress derived by rigid column idealization

in which the idea of rigid soil column is employed (Fig. 19.31) together with correction for deformation of real soil; r_d. The factor, r_d, is a function of depth, z (*meter*), (Figs. 19.4 and 19.32) and many response analysis by complex-modulus models found it approximated by

$$r_d = 1 - 0.015z \quad \text{or} \quad r_d = 1 - 0.025z \qquad (19.13)$$

Consequently, the cyclic stress ratio in subsoil is given by

$$\frac{\tau_{cy}}{\sigma'_{vo}} = \frac{\dfrac{A_{max}\left(\text{weight of soil}\right)}{g} \times r_d}{\text{weight of soil - buoyancy}} = \frac{A_{max}\sigma_{vo}r_d}{g\sigma'_{vo}} \qquad (19.14)$$

Equation (19.13) is going to be examined here against a the which the displacement amplitude is given by

$$u = 2E\cos\frac{\omega z}{V_s}\cos\omega t \qquad (19.15)$$

(see Sect. 4.4 and Exercise 1). The amplitude of cyclic shear st

$$\tau_{cy} = G\left|\frac{\partial u}{\partial z}\right|_{\text{amplitude}} = G\frac{2E\omega}{V_s}\sin\frac{\omega z}{V_s} \qquad (19.16)$$

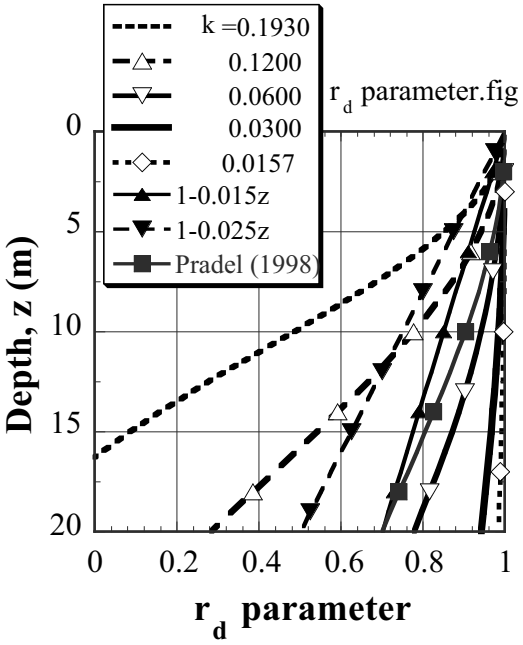

Fig. 19.32 Comparison between empirical "r_d" functions with harmonic response analyses

while the acceleration amplitude at the surface, A_{max}, and the weight of soil above *z* are derived as

$$A_{max} = 2\omega^2 E \quad \text{and} \quad \text{weight of soil} = \rho g z \qquad (19.17)$$

Consequently, r_d in (19.31) is expressed as

$$r_d = \frac{\tau_{cy}g}{A_{max}\sigma_{vo}} = \frac{G\dfrac{2E\omega}{V_s}\sin\dfrac{\omega z}{V_s} \times g}{2\omega^2 E\rho g z} = \frac{\sin\dfrac{\omega z}{V_s}}{\dfrac{\omega z}{V_s}} \qquad (19.18)$$

Equations (19.13) and (19.18) are compared for cases below;

Low frequency and dense sand: 0.5 Hz $\rightarrow$ $\omega = \pi$ and SPT-N=15 $\rightarrow$ $V_s = 80\ N^{1/3}$=200 m/s. Hence,

$$k \equiv \omega / V_s = 0.0157.$$

Higher frequency at liquefaction and loose sand: 4 Hz $\rightarrow$ $\omega = 8\pi$ and $N = 4$ $\rightarrow$ V_s=130 m/s. Hence,

$$k = 0.193.$$

Figure 19.32 illustrates the r_d parameters when k varies between these two extreme values. How do you feel about this figure? Pradel (1998) proposed $r_d = 1 \Big/ \left\{1 + \left(z/30.5\right)^2\right\}$.

19.12 Effects of Multi-Directional Shear on Liquefaction Resistance

Real earthquake motions in the horizontal direction consist always of EW and NS components, which exert subsoils two components of cyclic shear stress. It seems, therefore, that real earthquake conditions are more likely to induce liquefaction than laboratory idealization that exerts only one component of shear stress.

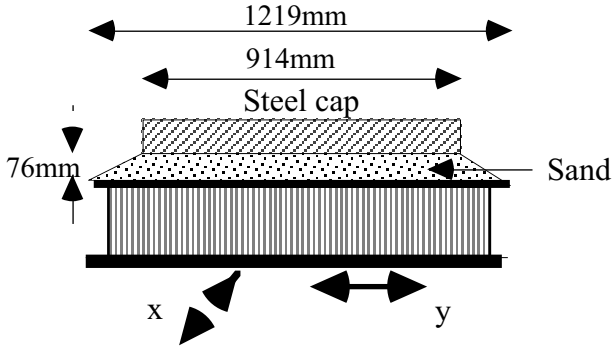

Fig. 19.33 Simple shear shaking table test (after Pyke et al. 1975)

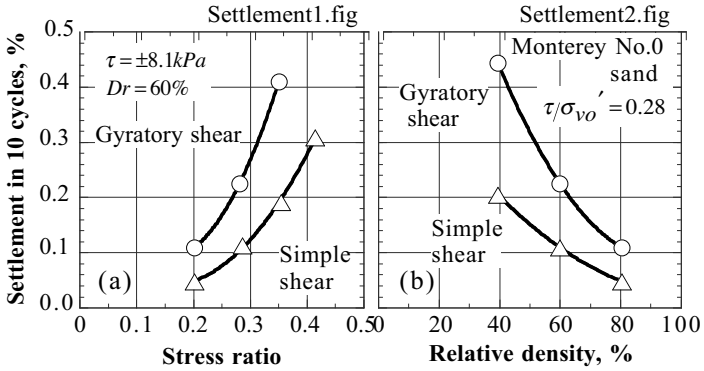

Fig. 19.34 Volume contraction of dry sand subjected to two-directional gyratory shear and one-directional simple shear (Pyke et al. 1975)

Pyke et al. (1975) carried out large simple shear tests on a two-directional shaking table (Fig. 19.33, see Sect. 19.7). The combination of EW and NS motions induced a greater volume contraction of dry tested sand than individual components did (Fig. 19.34) and, hence, it was expected that the two-directional shaking can induce liquefaction more easily than shaking in only one direction (Seed et al. 1978).

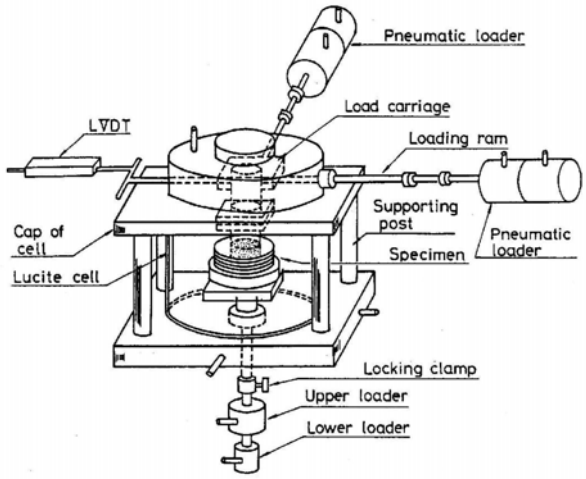

Fig. 19.35 Two-directional simple shear device (Ishihara and Yamazaki, 1980)

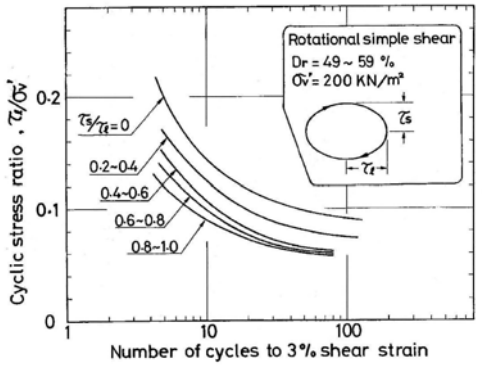

Fig. 19.36 Effects of multi-directional shear on liquefaction resistance of sand (Ishihara and Yamazaki, 1980)

Ishihara and Yamazaki (1980) conducted two-directional undrained simple shear tests (Fig. 19.35). Figure 19.36 indicates that the stress ratio needed to cause 3% shear strain decreases as the magnitude of the second component of shear stress, τ_s, increases. Consequently, Fig. 19.37 manifests that the correction factor, C_5 in Sect. 19.4, for the multidirectional shaking becomes more important as the ratio of the minor and the major shear stresses, τ_s/τ_1, approaches one.

Experimental studies have so far shown that, in case that there is no initial static shear, the two-

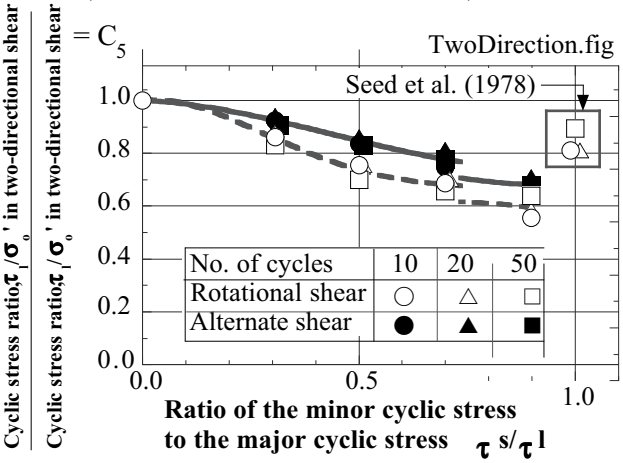

Fig. 19.37 Correction of liquefaction resistance of sand in terms of multi-directional shaking (Ishihara and Yamazaki, 1980)

dimensional loading induces volume contraction or triggers liquefaction more easily than conventional one-dimensional loading (Pyke et al. 1975; Seed et al. 1978; Ishihara and Yamazaki, 1980; Kammerer et al. 2004). This certainly implies that negative dilatancy (volume contraction due to shear) is increased by two-dimensional loading. This issue was further indicated experimentally by running drained two-dimensional shear. Figure 19.38 illustrates an experimental device, which generates two-directional simple shear loading on sand.

Tests were performed on dense sand that normally exhibits volume expansion during shear. Figure 19.39 shows the volume change during shear. Since the relative density of the specimens exceeded 100%, volume expansion or positive dilatancy was going to start in the phase of monotonic shear in the x direction (between the origin and ○). When superposition of the cyclic loading in the y direction was initiated at the points of ○, however, a significant extent of volume contraction (positive volumetric strain) started. This transition from positive dilatancy to negative one (volume contraction) is equivalent in undrained shear with higher pore water pressure and greater deformation. Thus, although positive dilatancy in conventional one-dimensional loading exhibited the development of rigidity and shear strength in undrained conditions (Sect. 18.7), two-dimensional loading may drastically change this situation.

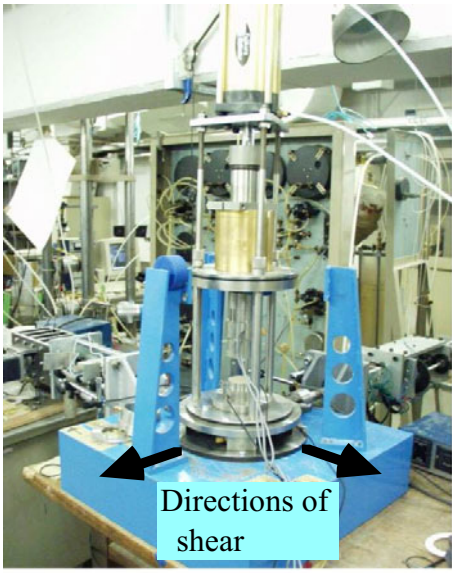

Fig. 19.38 Two-directional simple shear apparatus (Horie, 2000)

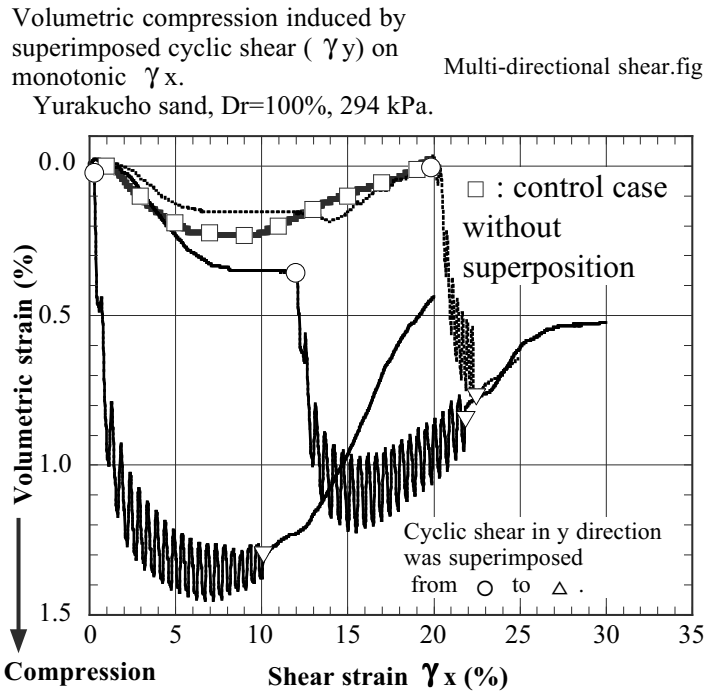

Fig. 19.39 Volume change of dense sand specimen undergoing multidirectional simple shear (Horie, 2000)

19.13 Grain Size Distribution of Liquefaction-Prone Sand

It has been conventionally considered that fine sand with uniform grain size (clean sand) is highly susceptible to liquefaction. In contrast, gravelly soil and silty materials have been regarded as less liquefiable (see Sects. 20.2, 20.4, and 20.5). The ideas behind this have been as what follows:

1. Gravelly soil has high permeability. Therefore, the excess pore water pressure would dissipate quickly so that no time would be available for large ground deformation to occur.
2. Upon water sedimentation of soil, small sand grains sink more slowly than gravels due to viscous resistance of water (Stokes law). Slow velocity of sedimentation leads to loose grain packing (Kolbuszewski, 1948a, b).
3. Cohesion in silty soil prevents development of large deformation during strong shaking (Sect. 20.4).

These remarks suggest the high liquefaction risk of fine loose sand in which permeability is low due to its small grain size and there is no cohesion. Accordingly, Fig. 19.40 has been widely accepted as the range of grain size distribution of potentially liquefiable sand. Compare Fig. 19.40 with Fig.19.41, which was obtained from silty sand that liquefied during the 2000 Tottoriken Seibu earthquake (Sect. 17.10).

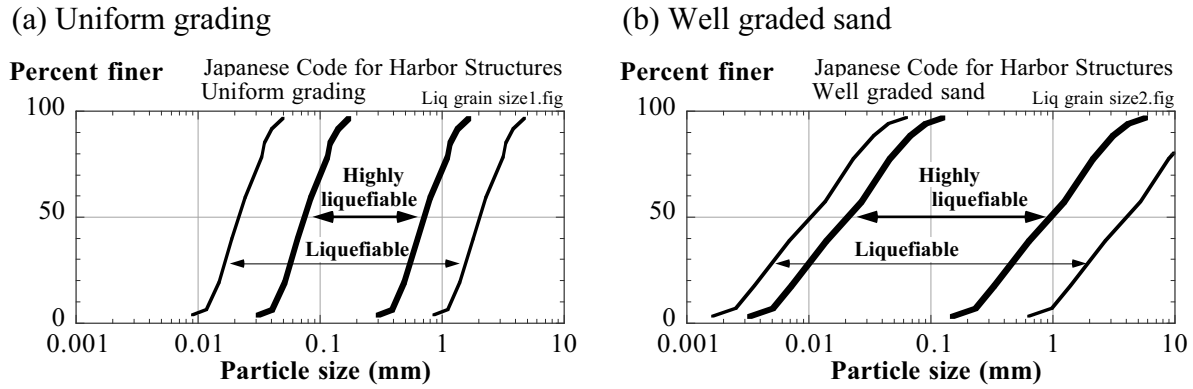

Fig. 19.40 Example of grain size distribution of liquefaction-prone sand (Japanese Seismic Code for Harbor Structures)

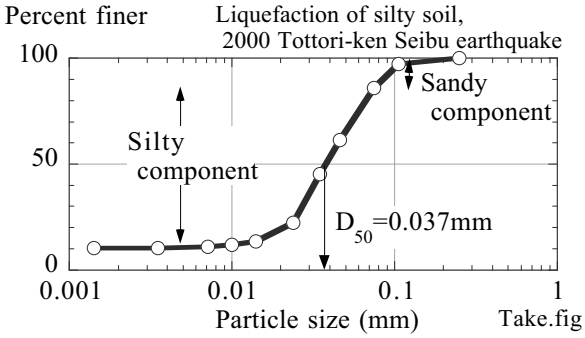

Fig. 19.41 Grain size distribution of liquefied silty sand

The three issues stated earlier are not the case under the following situations.

1. A loose and water-saturated gravelly deposit is covered by an impervious silty layer, which prevents seepage and dissipation of excess pore water pressure (Kokusho et al. 1995). Surface pavement has similar effects (Fig. 20.9).
2. Void space among gravel particles is filled with loose and water-saturated sand.
3. Fine silty material has no cohesion. This is the case of tailing materials that are made of crushed stones (Sect. 20.5). Since the grain size is very small, permeability is low as well and pore pressure dissipation is made very difficult within a limited time.

Under such circumstances, liquefaction risk has to be taken into account. Since such materials are not common targets of study, it is desirable to investigate their liquefaction resistance by means of laboratory tests on undisturbed samples in place of using any empirical formula.

List of References in Chapter 19

Annaki, M. and Lee, K.L. (1977) Equivalent uniform cycle concept for soil dynamics, Proc. of ASCE, Vol. 10, GT6, pp. 549–564.

Arango, I. (1996) Magnitude scaling factors for soil liquefaction evaluations, J. Geotech. Geoenviron. Eng., ASCE, Vol. 122, No. 11, pp. 929–936.

Cole, E.R.L. (1967) The behaviour of soils in the simple-shear apparatus, Ph.D .Thesis, Cambridge University.

De Alba, P., Seed, H.B. and Chan, C.K. (1976) Sand liquefaction in large-scale simple shear tests, Proc. ASCE, Vol. 102, GT9, pp. 909–927.

Federal Highway Administration (1997) Design Guidance: Geotechnical Earthquake Engineering for Highways, Vol. 1, Design Principles, p. 123.

Finn, W.D.L., Bransby, P.L. and Pickering, D.J. (1971) Sand liquefaction in triaxial and simple shear tests, Proc. ASCE, Vol. 97, SM4, pp. 639–659.

Horie, Y. (2002) Study on behavior of soil subjected to cyclic loading by simple shear test and site investigation, Master thesis, University of Tokyo.

Ishihara, K. and Li, S. (1972) Liquefaction of saturated sand in triaxial torsion shear test, Soils Found., Vol. 12, No. 2, pp. 19–39.

Ishihara, K. and Takatsu, H. (1979) Effects of overconsolidation and K_0 conditions on the liquefaction characteristics of sands, Soils Found., Vol. 19, No. 4, pp. 59–68.

Ishihara, K. and Yamazaki, F. (1980) Cyclic simple shear tests on saturated sand in multi-directional loading, Soils Found., Vol. 20, No. 1, pp. 45–59.

Ishihara, K. and Yasuda, S. (1975) Sand liquefaction in hollow cylinder torsion under irregular excitation, Soils Found., Vol. 15, No. 1, pp. 45–59.

Ishihara, K. and Yamazaki, F. (1980) Cyclic simple shear tests on saturated sand in multi-directional loading, Soils Found., Vol. 20, No. 1, pp. 45–59.

Japanese Society of Soil Mechanics and Foundation Engineering (Former name of Japanese Geotechnical Society) (1988) Proc. Symp. Undrained Cyclic Tests on Soils, Committee Report, p. 23 (in Japanese).

Kammerer, A.M., Seed, R.B., Wu, J., Riemer, M.F. and Pestana, J.M. (2004) Pore pressure development in liquefiable soils under bi-directional loading conditions, Proc. 11th Int. Conf. Soil Dynamics and Earthquake Engineering and the 3rd Int. Conf. Earthq. Geotech. Eng., Berkeley, Ed. T. Nogami and R.B. Seed, Vol. 2, pp. 697–704.

Kokusho, T., Tanaka, Y., Kawai, T., Kudo, K., Suzuki, K., Tohda, S. and Abe, S. (1995) Case Study of rock debris avalanche gravel liquefied during 1993 Hokkaido-Nansei-Oki Earthquake, Soils Found., Vol. 35, No. 3, pp. 83–95.

Kolbuszewski, J.J. (1948a) General investigation of the fundamental factors controlling loose packing of sands, Proc. 2nd Int. Conf. Soil Mech. Found. Eng, Vol. 1, pp. 47–49.

Kolbuszewski, J.J. (1948b) An experimental study of the maximum and minimum porosities of sands, Proc. 2nd Int. Conf. Soil Mech. Found. Eng, Vol. 1, pp. 158–165.

Lee, K.L. and Chan, K. (1972) Number of equivalent significant cycles in strong motion earthquakes, Proc. Int. Conf. Microzonation for Safer Construction Research and Application, pp. 609–627.

Lee, K.L. and Seed, H.B. (1967) Cyclic stress conditions causing liquefaction of sand, Proc. ASCE, Vol. 93, SM1, pp. 47–70.

Lee, K.L. and Seed, H.B. (1967) Dynamic strength of anisotropically consolidated sand, Proc. ASCE, Vol. 93, SM5, pp. 169–190.

Pradel, D. (1998) Procedure to evaluate earthquake-induced settlements in dry sandy soils, J. Geotech. Geoenviron. Eng., ASCE, Vol. 124, No. 4, pp. 364–368.

Pyke, R., Seed, H.B. and Chan, C.K. (1975) Settlement of sands under multidirectional shaking, Proc. ASCE, Vol. 101, GT4, pp. 379–398.

Seed, H. B., Idriss, I. M. and Arango, I. (1983) Evaluation of liquefaction potential using field performance data. Proc. ASCE, Vol. 109, GT3, pp. 458–482.
Seed, H.B. and Idriss, I.M. (1971) Simplified procedure for evaluating soil liquefaction potential, Proc. ASCE, Vol. 97, SM9, pp. 1249–1273.
Seed, H.B. and Idriss, I.M. (1982) Ground motions and soil liquefaction during earthquakes, Earthq. Eng. Res. Inst., ISBN 0-943198-24-0, p. 110.
Seed, H.B., Pyke, R.M. and Martin, G.R. (1978) Effect of multidirectional shaking on pore pressure, Proc. ASCE, Vol. 104, GT1, pp. 27–44.
Vaid, Y.P. and Chern, J.C. (1985) Confining pressure, grain angularity, and liquefaction, J. Geotech. Eng., ASCE, Vol. 111, No. 10, pp. 1229–1235.
Vaid, Y.P. and Finn, W.D.L. (1979) Static shear and liquefaction potential, Proc. ASCE, Vol. 105, GT10, pp. 1233–1246.
Yokouchi, N. (1997) Undrained torsion shear on dense sand subjected to strong earthquake loading, Bachelor thesis, University of Tokyo.